



TITLE:

# An Analysis of Strong Motion Accelerograms near the Epicenter

AUTHOR(S):

IRIKURA, Kojiro; MATSUO, Kazuko; YOSHIKAWA, Soji

---

CITATION:

IRIKURA, Kojiro ...[et al]. An Analysis of Strong Motion Accelerograms near the Epicenter. Bulletin of the Disaster Prevention Research Institute 1971, 20(4): 267-288

ISSUE DATE:

1971-03

URL:

<http://hdl.handle.net/2433/124799>

RIGHT:

# An Analysis of Strong Motion Accelerograms near the Epicenter

By Kojiro IRIKURA, Kazuko MATSUO and Soji YOSHIKAWA

(Manuscript received February 4, 1971)

## Abstract

The strong motion accelerograms of the Matsushiro earthquake were analyzed by various methods. When the velocity and the displacement in the time domain and in the frequency domain are calculated from the accelerogram, various errors may be introduced. Therefore, it is necessary to check and select the methods of data processing according to the purpose of analyses. In this paper, it was shown that the comparison of observed values with theoretical in the form of velocity amplitude spectral density might be most preferable. The main factors affecting the ground vibration during disastrous earthquakes are generally conceived to be: source, path and local geology. The relations between the observed seismogram and the theoretical one were compared when a moving dislocation model was assumed. It was found that the direction of particle motion and the spectral density of observation could be reasonably understood from the theoretical point of view.

## 1. Introduction

To obtain the main physical parameters of strong earthquake motion, the accelerograms of the Matsushiro swarm earthquakes were analyzed as much information in regard to the geological conditions and focal mechanisms is well known. The accelerograms used for the analyses are those of the Matsushiro earthquake published by the Strong Motion Observation Center of the Tokyo Earthquake Research Institute and Public Works Research Institute, Ministry of Construction. These accelerograms of the strong earthquakes in Matsushiro were obtained at the epicentral distance 1-10 km whose magnitude was 4-5.

In this paper, the relevant physical characteristics of the strong earthquake motion are investigated by obtaining the true ground velocity and displacement through integration of the accelerograms and Fourier spectrum of the strong motion. It is necessary to consider the type of source, relative positions between sites and sources, types of waves and their attenuation during transmission, and multiple wave reflection as factors of strong ground motions. It is generally known that some variations may be observed according to the techniques of data handling in the case of analysis of strong motion accelerograms. In the first part of this paper are discussed the data processing methods used for strong motion accelerograms so as to get most accurately the ground velocity and displacement. The effects of errors in interpreting accelerograms which are used for calculating velocities, displacement and Fourier spectra, must be considered. Error may be caused by small random reading errors, centerline adjustment, setting of initial value, chart paper distortion etc.

In particular, when double integration of accelerograms to obtain ground displacements is carried out, more care must be given to the methods used, since the displacement results may be significantly altered for some parts of the frequency spectrum. The errors associated with this procedure have been discussed in detail by Schiff and Bogdanoff (1967), Hudson, Nigam and Trifunac (1969) etc. Schiff and Bogdanoff (1967) concluded that at the present time, the use of an accelerogram to determine the net displacement is impractical. However, the optimum data processing method should be determined according to the purpose of the analysis. The integration is carried out both in the time domain and the frequency domain, and these are mutually checked to minimize the effect of errors caused by zeroline and digitizing.

In the latter part, the theoretical seismic spectral density and seismograms are numerically calculated and the results are compared with those of the observed data. The earthquake motions near the source depend chiefly on the source time function; moreover the effect of amplification by the soft surface layers has to be considered.

## 2. The Data Processing of Accelerograms

The observation points and the specifications of strong motion accelerograms for the Matsushiro earthquakes are noted in detail in references 3 and 4. The characteristics of the instruments are shown in Table 1. The locations of epicenters of the earthquakes analyzed in this paper and the observation points are shown in Fig. 1. The magnitude, focal depth, epicentral distances, intensity and maximum accelerations are shown in Table 2. The digitizations of the analog data were made by comparator manually.

The procedures of calculating velocity and displacement in the time domain are as follows. 1. The accelerograms were digitized at equal intervals of 0.025 cm (ca. 0.025 sec), and 7~12 cm in recording length. The samplings of equal intervals on the record papers

Table 1. Characteristics of the strong motion seismograph.

	SMAC-B <sub>2</sub>	DC-3C
Natural period	0.14 sec	0.1 sec
Sensitivity	12.5 gals/mm	25 gals/mm
Damping	critical	critical
Recording range	10~500 gals	10~1000 gals
Recording speed	10 mm/sec	10 mm/sec

Table 2.

	No. 147 May 28, '66			No. 300 Aug. 20, '66			No. 301 Aug. 20, '66		
	M 4.7 D 3.2 km			M 4.4 D 3.5 km			M 4.4 D 5.1 km		
	Dist.	I	Max. Ac.	Dist.	I	Max. Ac.	Dist.	I	Max. Ac.
Matsushiro C	1.6 km	V	0.37 g	2.1	IV	0.17	2.5	IV	0.13
Kawanakajima	5.5	V	0.20	6.2	IV	0.26	5.5	IV	0.30
Mashima	3.8	IV	0.13	3.1		0.14	2.7		0.27
Ochiai Bridge	6.5		0.10						
Susobana Dam	13.0		0.053						

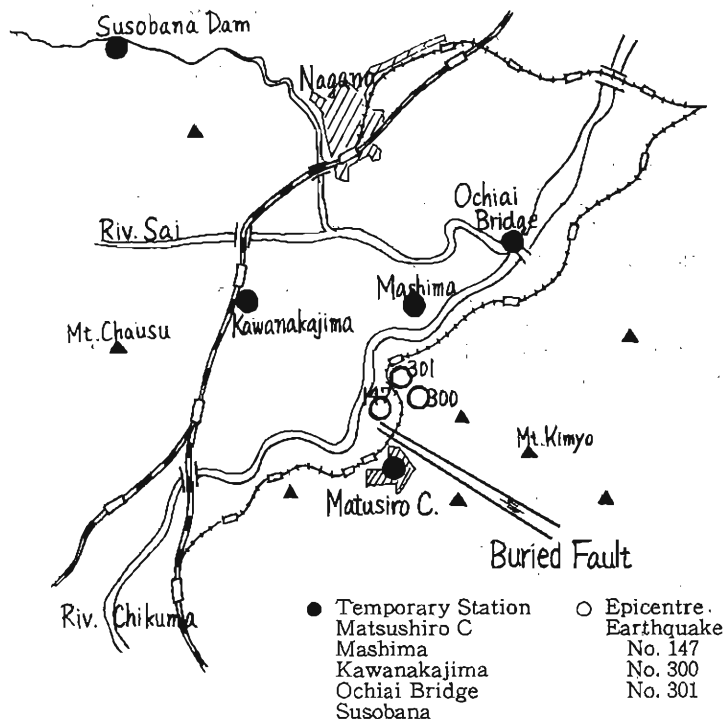


Fig. 1. Rough map of the vicinity of Matushiro.

result in unequal time digitization. 2. The zeroline was corrected assuming an apparent straight line as the zeroline on the record. 3. Circular arc movements of the pen were corrected. 4. Using Lagrange's interpolation formula (4 points) 2<sup>n</sup> equal time data were made. A high cut filter, cut off frequency 5cps and 30db down at 10cps, was applied to suppress the disturbances in the high frequency components. 5. Zeroline correction was made so as to minimize the mean square value of the ground velocity. In this case the shape of the acceleration zeroline was taken as either a straight line or a parabola line. 6. True ground acceleration was obtained considering the characteristics of the accelerograph. 7. Velocity and displacement were calculated by numerical integration. The initial conditions of velocity and displacement were to be duly determined.

#### Digitization Error

The resolving power of the comparator is 0.05 mm, but we find by repeated reading that the maximum error will be about 0.2 mm. The maximum amplitudes on the record used for the analysis were 10~20 mm and hence the digitization errors will be less than 2%. Schiff estimated the standard deviation of calculated velocity and displacement, assuming the digitization error to be a Gaussian noise whose mean value is zero and standard deviation  $\sigma$ . The standard deviation of velocity is given by  $(T/N^{\frac{1}{2}}) \cdot \sigma$  and that of displacement  $0.645 (T^2/N^{\frac{1}{2}}) \cdot \sigma$ , where  $\sigma$ : standard deviation of reading

error of accelerogram,  $T$ : record length,  $N$ : number of sampling. In this calculation,  $T$  is about 10 sec,  $N$  is 512 and then the standard deviation of velocity is about  $0.5 \cdot \sigma$ , and that of displacement about  $3 \cdot \sigma$ . Hence the digitization error effects on the velocity are rather small and those on the displacement are also not significantly large.

### Zeroline Correction

The zero acceleration level is not indicated on the record. The difficulties in determining the zeroline position have been discussed. For instance, (1) The initial parts of the shock are not recorded and hence the initial values of velocity and displacement can not be known. (2) A distortion of the paper record may be caused by the accelerograph transport mechanism, and it can not be expressed as a time function. The center line is usually assumed to take the form  $C_0 - C_1t - C_2t^2$  and to be given by the following equations respectively.

$$a(t)_{\text{corr}} = a(t) - (C_0 - C_1t - C_2t^2)$$

$$v(t)_{\text{corr}} = v(t) - (k - C_0t - C_1/2t^2 - C_2/3t^3).$$

In relation to the records used for the analysis, we could not find the optimum method for selecting each coefficient. Several Fourier spectra corresponding to the various methods of zeroline correction are shown in Fig. 2-4, and the calculated velocities and displacements in this case are shown in Fig. 5-7. Case 1. The correction is carried out by the apparent zeroline on the accelerogram (—line), taking  $C_2=0$ . Case 2. The curve is evaluated considering the initial value of the velocity, and to minimize the mean square computed ground velocity, taking  $C_2=0$  (---line). Case 3. Assuming the zeroline of the accelerogram as a parabola, the curve is obtained to minimize the velocity when the initial value of the velocity is zero (---line). Case 4. The curve is evaluated including the initial value by the same process as case 3 (.....line).

The optimum criteria in cases 1-4 should be determined according to the purpose of the analysis. The differences of the Fourier spectra in the low frequency range below

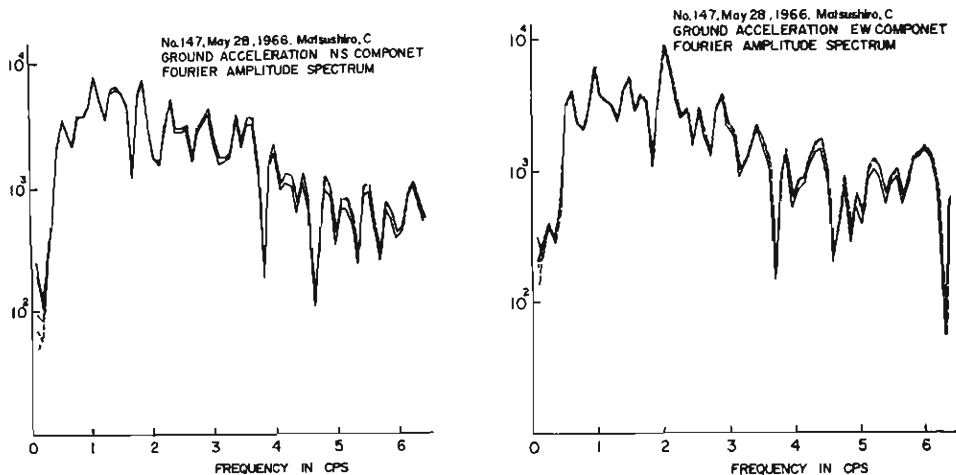


Fig. 2. Effect of zero line adjustment on Fourier spectrum (Matsushiro C).

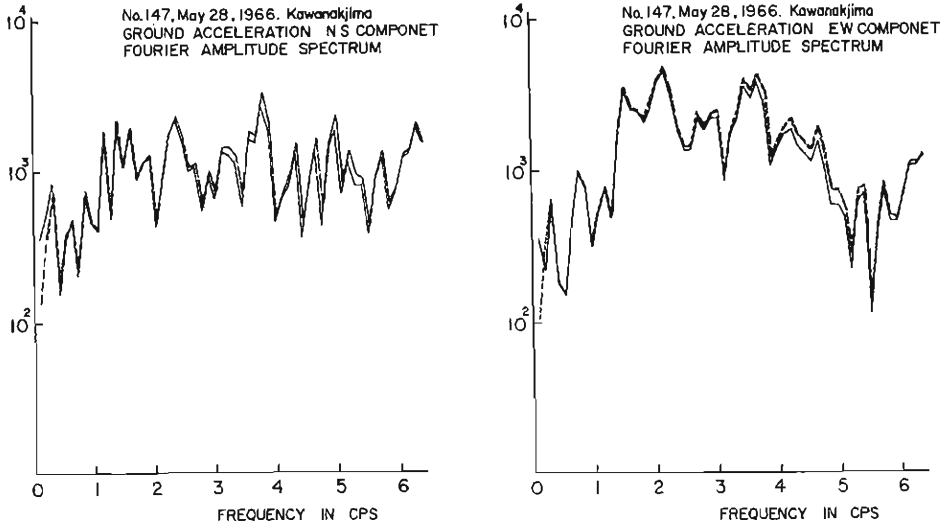


Fig. 3. Effect of zero line adjustment on Fourier spectrum (Kawanakajima).

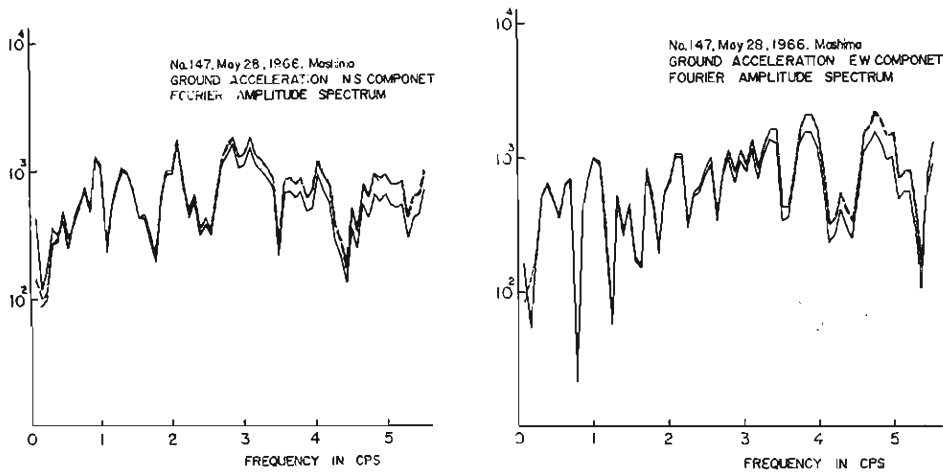


Fig. 4. Effect of zero line adjustment on Fourier spectrum (Mashima).

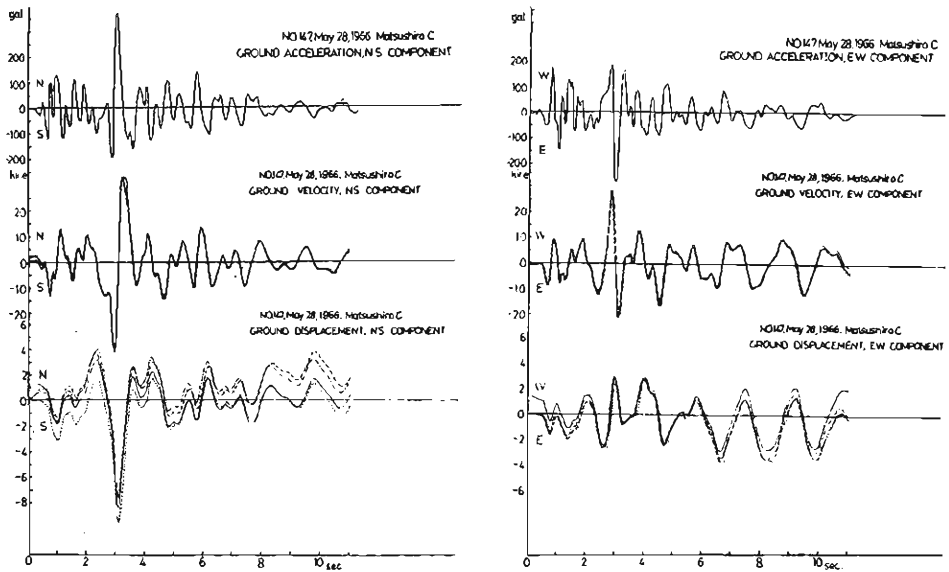


Fig. 5. Effect of zero line adjustment on calculated velocity and displacement (Matsushiro C).

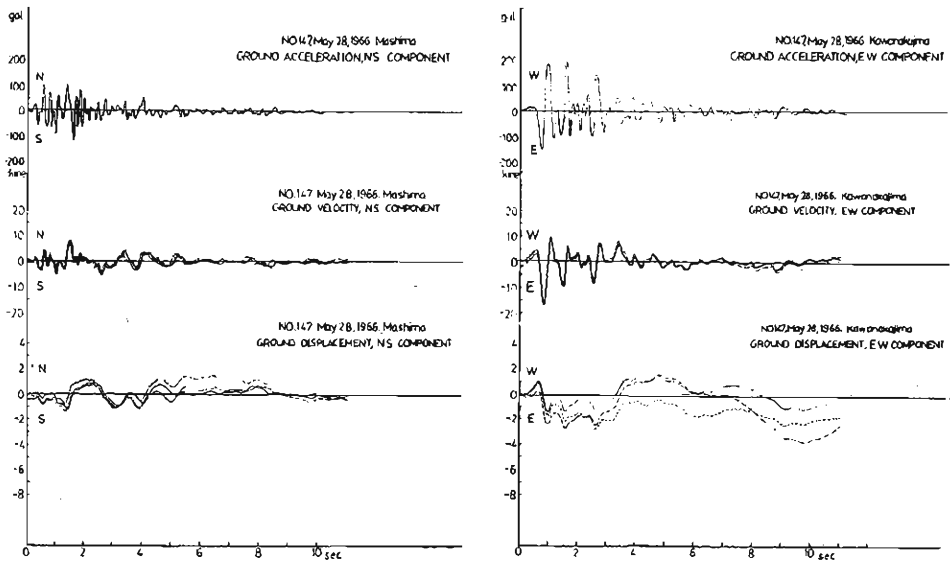


Fig. 6. Effect of zero line adjustment on calculated velocity and displacement (Kawanakajima).

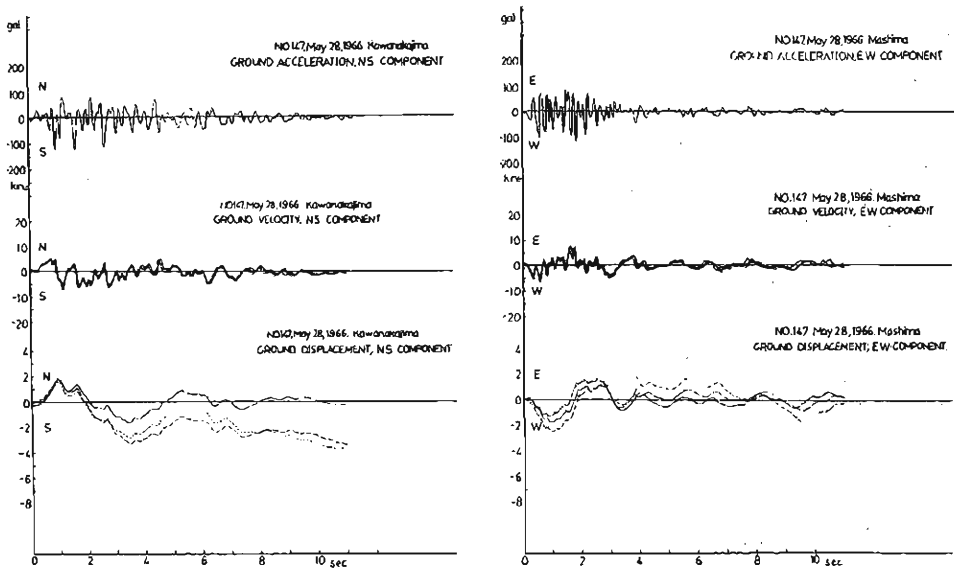


Fig. 7. Effect of zero line adjustment on calculated velocity and displacement (Mashima).

0.2 cps are comparatively large, but are negligible in other frequency ranges. The calculated velocity and displacement depend largely on the initial conditions. The error effect caused by center line correction is 5% of the velocity (about 1 kine) at its maximum. On the other hand, the maximum displacements differ from each other about 2cm according to the different zero correction methods, which are independent of the amplitude of the record. So the calculated displacement in this method can not be reliable for records whose maximum values are below 2cm.

The solid lines in Figs. 5-7 show velocity and displacement calculated in the frequency domain. Let  $x(t)$  be the observed ground acceleration corrected by the specification of the instruments; the Fourier transform is then given by:

$$f(\omega) = 2 \cdot \int_0^{\infty} \ddot{x}(t) \cdot e^{-i\omega t} \cdot dt \tag{1}$$

and the velocity is given by

$$\dot{x}(t) = \frac{1}{\pi} \cdot \int_0^{\infty} \frac{f(\omega)}{i\omega} \cdot e^{i\omega t} \cdot d\omega \tag{2}$$

and the displacement by

$$x(t) = -\frac{1}{\pi} \cdot \int_0^{\infty} \frac{f(\omega)}{\omega^2} \cdot e^{i\omega t} \cdot d\omega \tag{3}$$

The Fourier transform and inverse transform are carried out by the Cooley-Turkey algorithm. The standard deviation of the digitization error of the displacement is almost the same as that of the accelerogram from the calculation by Schiff's equation.



As shown in Fig. 2-4, the differences of the Fourier spectra are remarkable in the low frequency range below 0.2sec. It is apparent that the effect of errors in the low frequency range will be emphasized by integration, while the low frequency components of the observed accelerogram are small and the *S/N* ratio is very low. Therefore, it is essential to determine the frequency range in which the accuracy of calculation of the ground displacement may be at an acceptable level, in order to get the accuracy required. The calculations of velocity and displacement ((2) and (3)) were carried out by using the function in which the Fourier spectra  $f(\omega)$  of acceleration are multiplied by a weighting function which is flat above 0.33 cps and 30db down in the range of 0.33-0.0 cps, taking the forms of a Gaussian function. These results are shown in Fig. 5-7 by a full line. The transient time variation of the displacement in this method may be the most reliable, although the permanent displacement is not estimated. The displacement shown by the full lines in Fig. 5-7 is not zero when  $t=0$ , this may be elongated by filtering.

### 3. Characteristics of Earthquake Ground Motions

#### *Description of the Source Mechanism of the Matsushiro Earthquake and Buried Faults*

The source mechanism of the Matsushiro earthquake has been reported in detail from the seismological and geodetic point of view by many investigators.<sup>(6)</sup> The main compressional force has been inferred to be in an EW direction from the push-pull distribution of the initial motion of the *P* waves. And from the investigation of ground cracks a left lateral fault is inferred whose length is 7 km and whose direction is N55° W, horizontally displaced 42-57 cm. It is reported that these facts coincide well with the results of geodimetric observation and trigonometric survey. In Fig. 1 the distribution of ground cracks and the buried fault inferred by Tsuneishi and Nakamura<sup>10)</sup> are shown.

#### *Ground Acceleration, Velocity and Displacement*

The accelerogram used for the analysis was triggered by the earthquake motion and hence the initial parts of the *S* waves were sometimes recorded from the beginning. The ground velocity and displacement were calculated for the selected accelerograms in which the initial parts of the *S* waves were recorded. Calculated maximum

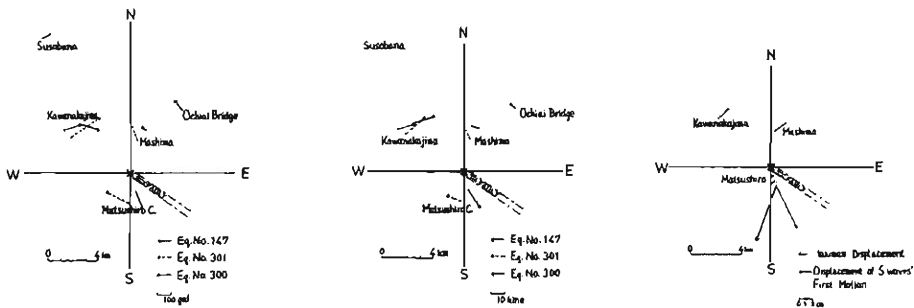


Fig. 8a. Particle acceleration. Fig. 8b. Particle velocity. Fig. 8c. Particle displacement.  
 Fig. 8. Vectors of *S* wave's initial motion.

displacements in Matsushiro, Kawanakajima and Mashima are 8.3 cm, 1.7 cm and 1.7 cm respectively. These values are rather small in comparison with the magnitude of their maximum accelerations.

To consider the relation between the source and the ground motion, the direction and amplitude of the initial  $S$  waves for earthquakes No. 147, 300 and 301 are shown in Fig. 8. Fig. 8-a shows the direction of particle acceleration, Fig. 8-b the particle velocity, and Fig. 8-c the particle displacement, respectively. The directions shown in Fig. 8 show a generally good agreement with that of the initial motion of the  $S$  waves when it is a double couple point source in EW main compressional force, excluding Matsushiro C; the area very near the epicenter should be checked in detail.<sup>(7)</sup> The calculations of displacement, velocity and acceleration wave forms in the near field of a propagating fault in a bounded medium are very difficult. Displacement, velocity and acceleration wave forms in the near field of a propagating fault have been computed numerically by Haskell.<sup>(8)</sup> It is interesting that the vector of the initial  $S$  waves and the maximum displacement vectors tend to coincide the ones which are deduced from his calculation, although the comparison is rather qualitative because his parameters cannot be applied to the Matsushiro earthquake directly.

Thus we have tried to estimate the theoretical spectrum and the seismogram by taking more appropriate parameters in the later section. The comparison of the observed velocity displacement with the theoretical one will be more preferable than that of the displacement, judging from the accuracy of the data processing results as shown in Fig. 5.

#### Fourier Spectra

The Fourier spectra of the accelerations shown in Fig. 2-4 are very complicated. The predominant frequency of micro-tremors reported by Kanai and et. al. is 2.5 cps

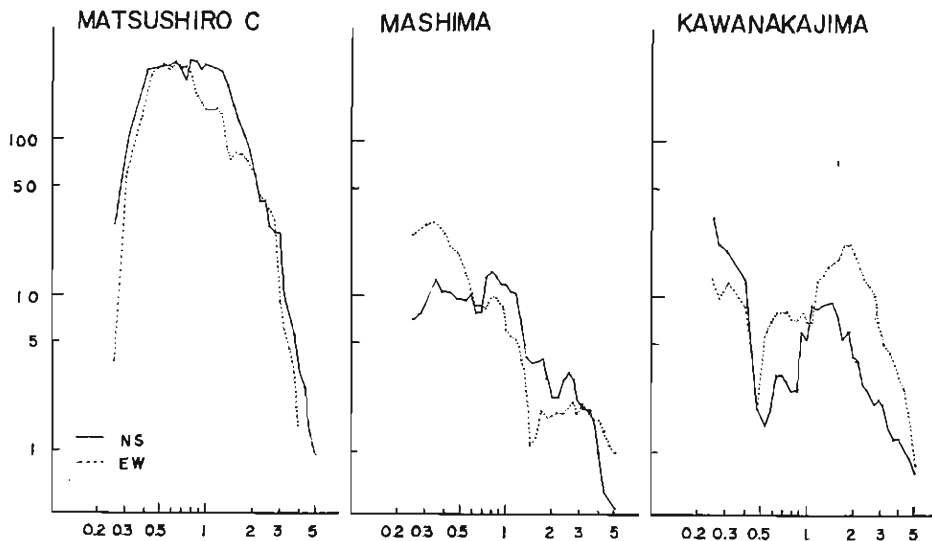


Fig. 9. Smooth energy spectral density of earthquake No. 147 at Matsushiro C, Kawanakajima and Mashima.

near Matsushiro C Station, 2~3 cps near Kawanakajima Station and 3 cps near Mashima Station. The relations between the spectral peaks and those of the micro-tremors are not always clear in Fig. 2-4.

Now we consider a method of smoothing the effect on the source and the complexity of the geological structure included in the spectra. Let  $E(\omega_0)$  be the energy of the earthquake in the frequency range between  $\omega_0 - k\omega_0$  and  $\omega_0 + k\omega_0$ ,  $k$  being the fractional constant. Then we get

$$E(\omega_0) = \frac{1}{2k\omega_0} \int_{\omega_0 - k\omega_0}^{\omega_0 + k\omega_0} \{\dot{u}(\omega)\}^2 \cdot d\omega \quad (4)$$

The calculated  $E(\omega)$  of each station for earthquake No. 147 ( $k = \frac{1}{4}$ , in this case) is shown in Fig. 9. The value of  $k$  should be determined in accordance with the purpose of the analysis. The energy spectra at any given stations are concentrated in the frequency range 0.3-2.0 cps. The peak of 2 cps in the Kawanakajima spectrum and the peak of 3 cps in that at Mashima are considered due to the effect of the ground structure. The spectrum at Matsushiro C Station has no peak presumed from the ground characteristics of the micro-tremor and makes a very simple shape. This means that the seismic spectra near the epicenter depend strongly on the source spectrum.

#### 4. Numerical Calculation of the Seismic Spectrum and the Synthesized Seismogram near a Dislocation Source

##### *Theoretical treatment*

The numerical calculations of the near field displacements around a propagating fault have been made in a somewhat different approach by Aki (1968) and Haskell (1969). Haskell has computed the displacement wave forms directly in the time domain by numerical integration of the Green's function integrates given by de-Hoop for the elastic field of a propagating fault in an infinite medium. Aki has taken the Fourier transforms of the integrates of the field due to a infinitesimal dislocation derived by Maruyama (1963), carried out a numerical integration over the fault plane to obtain the displacement spectrum, and finally returned to the time domain by Fourier synthesis. We have tried to compare the observational data with the theoretical data in both the frequency and the time domains and have made our numerical calculations by Maruyama's formula, similarly with Aki. The formula and the procedure used for calculation are summarized as follows.

The displacements  $u_m(q, t)$  at any point  $Q$  in an infinite homogeneous elastic medium due to the dislocation  $\Delta u_k(t)$  over a plane are given by equations 33 and 34 of Maruyama (1963),

$$u_m(Q, t) = \frac{1}{2\pi} \cdot \int_{-\infty}^{\infty} e^{i\omega t} \cdot d\omega \left\{ \int_{\Sigma} \Delta u_k(\omega) \cdot T_{kl}^m \cdot \nu_l \cdot d\Sigma \right. \quad (5)$$

$$\left. \Delta u_k(\omega) = \int_{-\infty}^{\infty} \Delta u_k(t) \cdot e^{-i\omega t} \cdot dt \quad (6) \right.$$

in which  $T_{kl}^m \cdot e^{i\omega t}$  is the  $m$ -component of the displacement field due to equivalent dynamic double forces acting along the  $k$ - and  $l$ -axes and is given by Maruyama's eq.

(35). (1963) The source depth of the Matsushiro earthquake is very shallow and hence strike slip dislocation is presumed as the source model. Therefore,  $\delta_{k1}=0$  in Maruyama's eq. (35). The higher order terms regarding distance  $r$  are calculated because near field displacements have to be estimated. In the coordinate shown in Fig. 10, letting the fault be in the  $x$   $y$ -plane, and considering the left-lateral, strike-slip dislocation on a vertical fault plane, then the  $x$ - and  $y$ -components at the observation point at  $Q$  are obtained by  $T_{zv}^z$  and  $T_{zv}^y$  respectively. The effect of a propagating dislocation along a fault is calculated by Ben-Menahem's approximation method. Let the transfer function be  $F$ , and we get

$$F = (\sin X_{p,s}) / X_{p,s} \cdot e^{-iX_{p,s}}, \quad (7)$$

where  $X_{p,s} = \omega L / 2v_{p,s} \cdot \left( \frac{v_{p,s}}{v} - \frac{y_Q - y_p}{R} \right)$ , and  $v$ ,  $v_p$  and  $v_s$  is the rupture velocity, the  $P$  wave's and  $S$  wave's velocity.

Let the dislocation  $\Delta u_{ij}$  be located in the fault element  $\Sigma_{ij}$  which is at the distance  $l$  from the initial dislocation point, then  $u_{ij}^m$  (the displacement of the observational point in the  $m$ -direction) is given by

$$u_{ij}^m = \Delta u_{ij}(\omega) \cdot T_{xy,ij}^m \cdot F_{ij}(\omega) \cdot \exp(-i\omega l/v) \quad (8)$$

The superposed displacement of the observation point is given by

$$u^m(\omega) = \sum_{i,j} u_{ij}^m(\omega) \quad (9)$$

and the velocity displacement by

$$\dot{u}^m(\omega) = u^m(\omega) / i\omega \quad (10)$$

The Fourier synthesis of (9) and (10) is made to get the displacement and velocity wave forms. This method can be applied only in the case of a homogeneous infinite medium, and hence may be used to compare the earthquake motions in the extreme neighborhood of the source in which the effect of complex short-period surface waves due to local shallow layered structure may be neglected. In the case of earthquake No. 147 observed at Matsushiro C the epicentral distance is 1.4 km, and its minimum distance to the buried fault found by Nakamura and Tsuneishi is less than 1 km. The observation stations at Kawanakajima and Mashima are located at the epicentral distances of 5-6 km, hence the comparisons between the observational data and the theoretical values are debatable. Therefore, the comparison is restricted in the case of Matsushiro C.

#### Assumed fault model

As indicated in Fig. 10, we assumed a rectangular fault of length  $L$  in the  $Y$  direction and width  $W$  in the  $Z$  direction. The time function of the dislocation was selected so as to coincide with the observational data considering both the cases of a step and of a ramp. Assuming a step as the time function of dislocation, its Fourier Transform  $\Delta u(\omega)$  is given by:

$$\Delta u(\omega) = D / i\omega \quad (11)$$

and in the case of a ramp by:

$$\Delta u(\omega) = (1/\omega^2 T)(e^{-i\omega T} - 1) \quad (12)$$

where  $D$ : amount of dislocation

$T$ : duration time

The amounts of  $D$  and  $T$  taken in this model are mean values over all the area of the fault. The length and width of the fault element is chosen on the basis of Aki's test of approximation method, and the fault is divided into  $40 \times 20$  elements. The length of the buried fault is reported to be about 7 km, however, it is very difficult to estimate which part of the fault is related to any individual earthquake. From observation of ultra-micro earthquakes it was reported that the aftershocks for two earthquakes of magnitude about 5 are spread over the area in an elliptical domain whose longer axis is about 7 km. (Hagiwara, et. al. 1967)

First, we assumed the length of the fault as 7 km and its width 3 km; and the calculation was carried out, and then the variation of the seismic spectrum due to the size of the fault was checked.

The epicenter of earthquake No. 147 is reported to be located at the north-west end of the buried fault. We have no other information about the propagation of the dislocation. Since the hypocenter may be located at the end of the buried fault, the propagation of the dislocation is assumed to be along the fault unilaterally from the north-west to south-east. The relative positions of the fault and the observation point are shown in Fig. 10. The coordinate of the observation point is assumed to be 0.8 km, 1.0 km and 0.0 km in the  $x$ ,  $y$  and  $z$  axes, respectively. The variations of the seismic spectrum in relation to the perpendicular distance are also checked in the range of 0.5~1.0 km.

According to the results of seismic prospecting carried out by the Explosion Group,

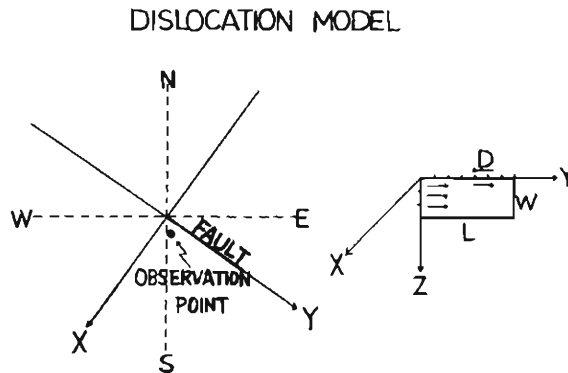


Fig. 10. Coordinate of observation point and fault plane geometry.

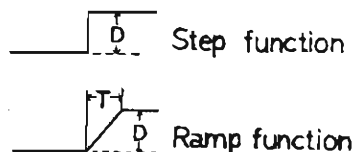


Fig. 11. Source time functions of the assumed dislocation model.

the  $P$  wave's velocity is about 6.0 km at the bed rock covered by a surface soft layer whose thickness is about 1 km. Assuming the Poisson ratio as  $\frac{1}{4}$ , the corresponding velocity of the  $S$  wave is 3.5 km/sec. The rupture velocity  $v$  in the  $y$ -direction is taken as  $v=0.75 \cdot v_s$ , given by Manshinha's formula. The rupture velocity in the  $z$ -direction is assumed to be infinity.

The effect of this soft layer (1 km in thickness) will be discussed later. As a first step the calculation of the seismic field in an infinite medium is made, taking the surface effect as factor 2; amplification caused by image source, because the near-field due to strike slip dislocation is conceived to be most predominant in the SH wave.

#### *Dependence of seismic spectrum on various source parameters*

The effect of source parameters on a seismic spectrum has been checked in detail by Aki who reported that the amount of dislocation affects the seismic spectrum mostly in the neighborhood of the hypocenter, while the total area of the fault surface, the fault depth and the rupture velocity do not affect it significantly. The earthquake analyzed was observed at a distance somewhat longer than 80 m in the case of the Parkfield earthquake of June 28, 1966.

We have very little information on the source parameter of Earthquake No. 147. Regarding ambiguous source parameters, we have to check the effect of each parameter on the earthquake motion, to find which is most effective when these values are varied in a plausible range. Hence the effects of the distance between observation point and fault, and of source size and source time functions on the seismic spectrum are investigated.

#### *The effect of source time function*

The time function of a dislocation is generally conceived to take step, ramp, and exponential forms. In this case strict discussion of the difference between the ramp and exponential forms is difficult, hence a step and a ramp are taken as the source time function. A step may be regarded as a ramp when its duration time  $T=0$ . In Fig. 12

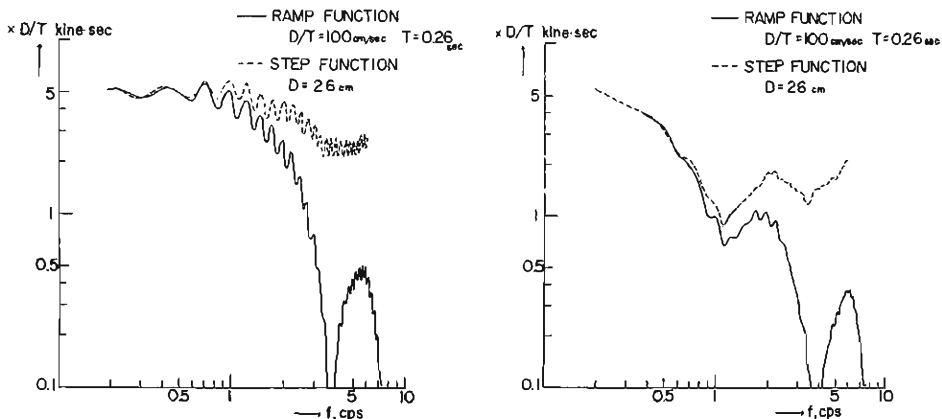


Fig. 12. The difference of the seismic velocity spectrum due to two assumed models of the source time function; assumed  $L=7$  km,  $W=3$  km,  $D=26$  cm,  $T=0.26$  sec and the coordinate of observation point (1.0, 1.0, 0.0). Left; perpendicular component. Right; parallel component.

the velocity spectral densities are shown when the dislocation is in the form of a step and of a ramp respectively. In the ordinate, the amount of density is shown as  $D$  which is the amount of dislocation, and in the abscissa the frequency is taken as a unit  $1/T$  which is the inverse of the duration time  $T$ . In the case of the ramp function the density takes a minimum value when  $1/T$ , while in the case of step no minimum value may be found and it is flat since it corresponds to  $T=0$ . The spectral density in the ordinate depends on the amount of dislocation in the low frequency range, and the position of the minimum in the abscissa is determined by  $1/T$ . Accordingly, when we get an ideal seismogram,  $D$  and  $T$  may be obtained by a parallel shift in the coordinate in which velocity spectrums are plotted in log-log scale. The displacement spectral density decays suddenly in the higher frequency range, and therefore the differences are not remarkable in the cases of both a ramp function and a step function.

#### *The effect of source size and distance*

In order to check the dependence of the source size on the seismic spectrum, four models are assumed.

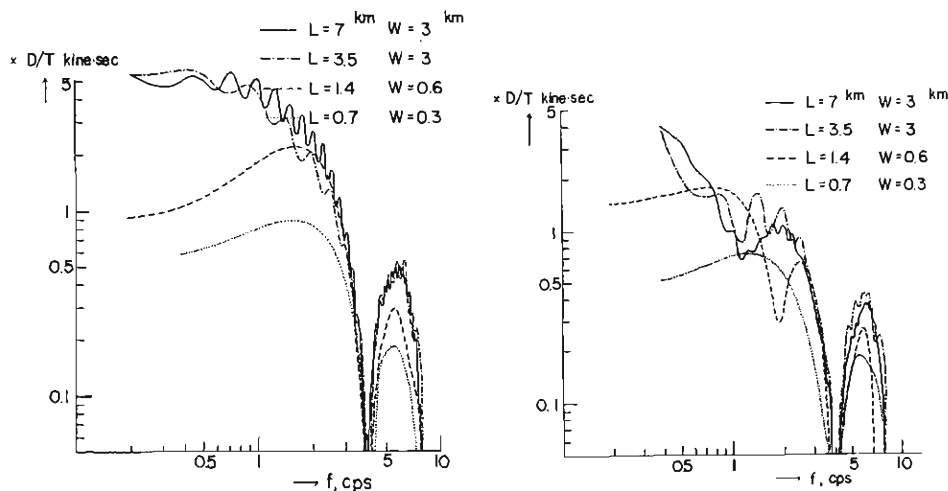


Fig. 13. The effect of source sizes on the seismic spectrum; assumed  $D=26$  cm,  $T=0.26$  sec, and the coordinates of the observation point (1.0, 1.0, 0.0).  
Left; perpendicular component. Right; parallel component.

- (1)  $L=7$  km,  $W=3$  km
- (2)  $L=3.5$  km,  $W=3$  km
- (3)  $L=1.4$  km,  $W=0.6$  km
- (4)  $L=0.7$  km,  $W=0.3$  km

Model (2) is  $1/2$  of model (1) in length; and (3), (4) resemble each other in shape, and their ratio of length and width to (1) is  $1/5$  and  $1/10$  respectively. Their spectra are shown in Fig. 13. The density values hardly decrease in the case of (2), and decrease  $1/3$  in (3) and  $1/10$  in (4) when compared with (1) in lower frequency range than 1 cps. The spectral density at a long distance is generally  $D \cdot L \cdot W$ , but even in the case model (4) it decreases only  $1/10$  when the fault size becomes  $1/100$ . The densities of (3) and (4) are small in the low frequency range, take their maximums at 1.6 cps

and decrease with the increase of the frequency. This may be regarded as an effect of the finiteness of the source area. The coincidence of peak frequency in (3) and (4) is supposed to be a superposition of the effects both of the finiteness of the source and the source time function. The observed spectrum is flat in the range from 0.5 cps to 2.0 cps and drops suddenly at higher frequencies and also decreases at lower frequencies. This drop of density at lower frequencies might be caused by the technique of analysis and observation or it might actually be the case. We have no clue to discriminate these effects. Consequently (3) and (4) are not applicable in this case, and the preference between (1) and (2) can not be determined easily.

The dependences of the spectrum on the minimum distances between the observation point and the fault when they are 0.5, 0.8 and 1.0 km are calculated and shown in Fig. 14. The variations of spectral densities in each case differ only by 50%, therefore, the distance of the fault do not affect the seismic spectral density most significantly in the range of 0.5 to 1.0 km.

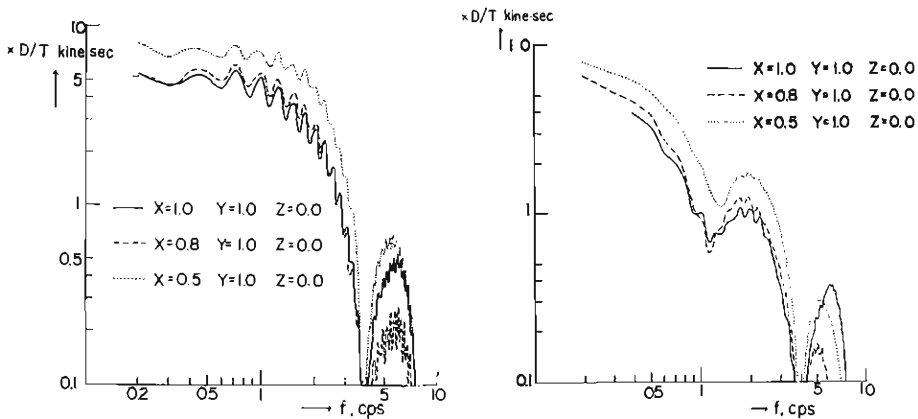


Fig. 14. The effect of distance from the fault; assuming the coordinates of observation point,  $x=0.5$  to  $1.0$  km,  $y=1.0$  km,  $z=0.0$  km, Assuming  $L=7$  km,  $W=3$  km,  $D=26$  cm and  $T=0.26$  sec. Left; perpendicular component. Right; parallel component.

#### Comparison between observed and theoretical velocity spectral density

The location of the fault and source parameters are assumed as follows, to verify the velocity spectral density of earthquake No. 147 observed at Matsushiro C as a reasonable model.

1. Assuming that the fault direction is  $N55^\circ W$ , the coordinate of the observation point is  $x=0.8$ ,  $y=1.0$ ,  $z=0.0$ .
2. The fault length;  $L=7$  km, width  $W=3$  km, rupture velocity  $v=2.7$  km/sec.
3. The source time function is a ramp.
4. Factor 2 is multiplied by the spectrum obtained under a homogeneous infinite medium as a surface effect.

The theoretical velocity spectrum is shown in Fig. 15 which is calculated on the above model. Comparing the shape of this theoretical velocity spectrum with that of observed one, it can be understood as follows.



1. The density decreases suddenly above the frequency of 2 cps.
2. The minimum value is found at 3.8 cps.

These two points resemble each other. The minimum is caused by the assumption of the duration time  $T=0.26$ . The choice of  $T=0.26$  sec is taken because the time interval between the maximum positive and negative velocity peaks is equal to the above value, which is found in the observed trace of the velocity displacement (shown in Fig. 5).

The observed velocity spectral density also takes a minimum value near 3.8 cps. As a matter of fact, many other peaks are found in the spectrum, but the minimum at 3.8 cps is most remarkable in the NS and EW components.

The theoretical spectra of the NS and EW components are different in shapes at frequencies lower than 2 cps. However, they resemble each other in shapes in the case of the observational data. Thus it may be expected that the actual direction will be near N45  $W$ . Assuming the direction of the fault to be N45  $W$ , the perpendicular distance to the fault is 0.5 km. In the above model the distance is changed to 0.5 km leaving the other parameters unchanged. The calculated spectral density is shown in Fig. 15 (dotted line). As may be seen in the figure, their forms resemble each other in the NS and EW components. This is more consistent with the observed data.

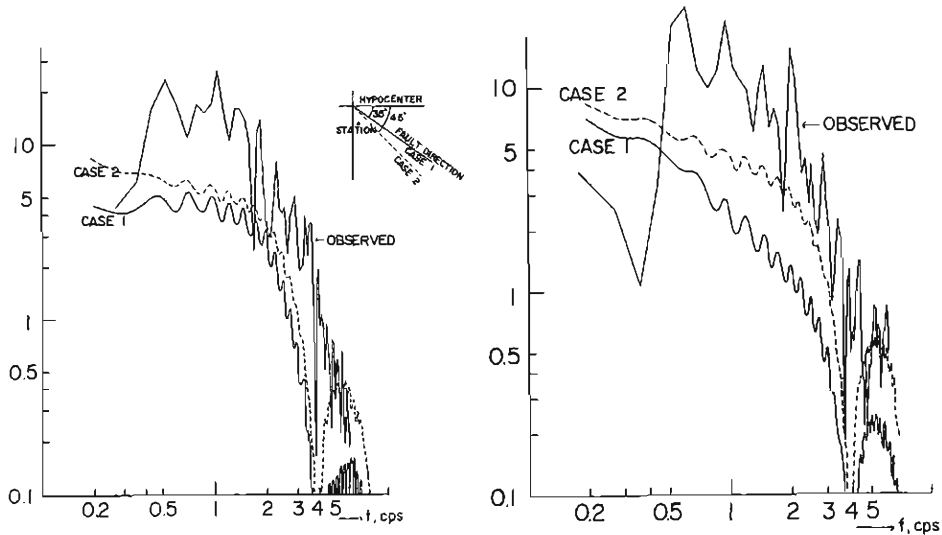


Fig. 15. Comparison between observed and theoretical velocity spectral densities. Case 1; assuming a fault direction of N35° W and observation point coordinates (0.8, 1.0, 0.0), Case 2; assuming a fault direction of N45° W and observation point coordinates (0.5, 1.0, 0.0). Left; NS component. Right; EW component.

Let us now compare the values of the spectral densities with those observed. Before direct calculation of  $D$ , the following facts are taken into consideration. Since  $D/T$  have the dimension of velocity, it may be regarded as independent of earthquake size (Aki, 1970). Aki pointed out that the  $D/T$  values were about 100 cm/sec which he obtained on the occasion of the Niigata Earthquake ( $M=7.8$ ) and the Parkfield Earthquake ( $M=6.4$ ), and they were independent of earthquake size. We have no other

detailed information on the length  $D$ ; assuming  $D/T=100$ cm/sec tentatively, we have compared the theoretical value of the spectral density with that observed. The observed value is 2~5 times larger than the theoretical one, when the above assumption is adopted.

The resulting difference might be caused by either a low estimation of  $D$ , the amount of dislocation, or by negligence of the amplification effect of the surface soft layers. First we have to consider the surface layers' effect as it is not taken into consideration in the theoretical calculation.

#### *The effect of the surface layer*

The buried fault may be regarded to exist under soft layer, hence the model adopted is contradictory to fact. In the above model, the spectrum corresponds to that of the base rock excluding the surface layer. In considering the effect of the surface layer, the drop of density caused by the sudden attenuation of the near-field terms resulting in the elongation of the distance corresponding to the thickness of the surface layer is conceived to be less than 50%, as shown in Fig. 14. This drop is smaller than the increase of density caused by multiple reflection in the surface layer.

The vibrational characteristics in layered media near the source are discussed in detail by Shima (1970) when the source is of the horizontal point source type. His calculations correspond to the transfer function of an earthquake motion which is excited by a horizontal point source at its base. According to his results the amplification by the surface layer is caused mainly by the multiple reflection of the SH wave, when the frequency is above ca. 0.5 cps.

The ground structure at Matsushiro C Station is obtained by seismic prospecting carried out by the Explosion Group and the  $P$  wave velocities of the several layers are given. The corresponding  $S$  wave velocities in the shallow layer are obtained referring to the results of our  $S$  wave prospecting in the vicinity of the Matsushiro region. On the other hand  $S$  wave velocities in the deeper layers might be assumed to be poisson ratio  $\sigma=\frac{1}{4}$ . From these results the  $S$  wave velocities at the observation point may be reasonably assumed and are shown in Table 3. Supposing the predominant waves radiated from the strike slip dislocation be SH waves, the amplification ratio caused by multiple reflection of these SH waves is computed and shown in Fig. 16.

The amplification characteristics at the surface calculated by the above assumption have several peaks, at 0.5cps, at 1.0cps, and etc, and these are 3~5 times larger than the amplification by the surface effect. This difference is of comparable order with that between the theoretical and observed values of the velocity spectral densities. When examining the velocity spectrum in detail, we find peaks at 0.5 cps and

Table 3. Geological structure.

	Thickness	P waves' velocity	S waves' velocity	Density
The first layer	0.3 km	2.0 km/sec	0.6 km/sec	1.8
The second layer	0.7	4.0	2.0	2.0
The third layer	—	6.0	3.5	2.6

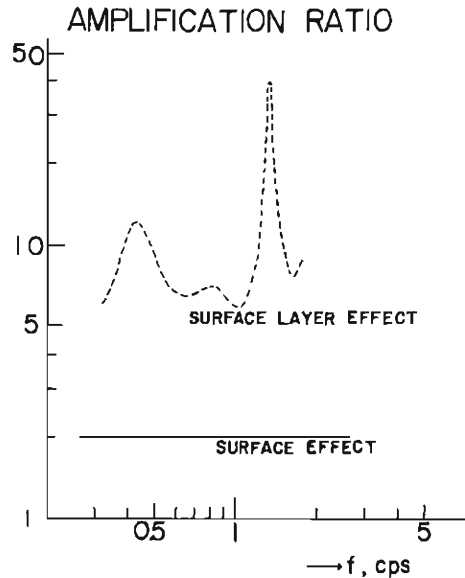


Fig. 16. Amplification effect of the seismic spectral density due to the surface and the soft surface layers.

1.0 cps in both the NS and EW components. At higher frequency ranges the effect of more precise geological micro-structure in shallow layers, attenuation of seismic waves and etc have to be considered. Although we tried very roughly to estimate the effect of surface soft layers, the peaks and the amplification of the spectral density are explained approximately.  $D/T=100$  is an assumption and not a unique solution, and nevertheless the coincidence between the theoretical and the observed values can be presumed to be validity of the value as an order estimation. Considering the ambiguities of the distance to the fault,  $D/T$  might be presumed to be 100~200 cm/sec.

#### *Synthesized seismograms*

The perpendicular and parallel components of synthesized seismograms of velocity are shown in Fig. 17. Fourier synthesis was made through the rectangular window (0.2-7.5cps). Because of the truncate effect the theoretical trace is not zero when  $t=0$ . The NS and EW components are shown in Fig. 18 making the transformation of the coordinate.

The forms of the observed seismograms are complicated and cannot be compared simply with the theoretical traces. As far as the portions of maximum amplitude are concerned, their shapes resemble each other. As regards the NS component of the theoretical trace, the maximum amplitude in the south direction equals  $0.125 \times D/T$  and is 12.5 kine when  $D/T=100$ .

Since the amplification due to the surface layer is presumed as about 4 times, the observed maximum amplitude of 35 kine coincides with the theoretical one as an order estimation.

However, this comparison neglects the time phase. Every phase on the observed

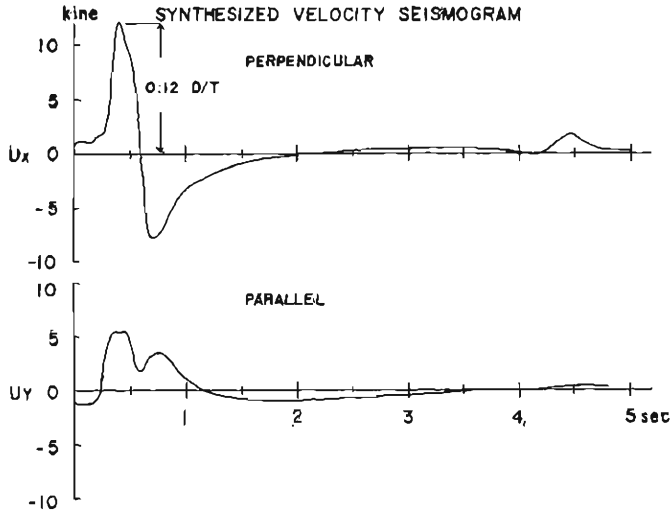


Fig. 17. Synthesized seismograms; perpendicular and parallel components to the fault. Assumed  $L=7$  km,  $W=2$  km,  $D=26$  cm,  $T=0.26$  sec and the observation point coordinates (0.5, 1.0, 0.0).

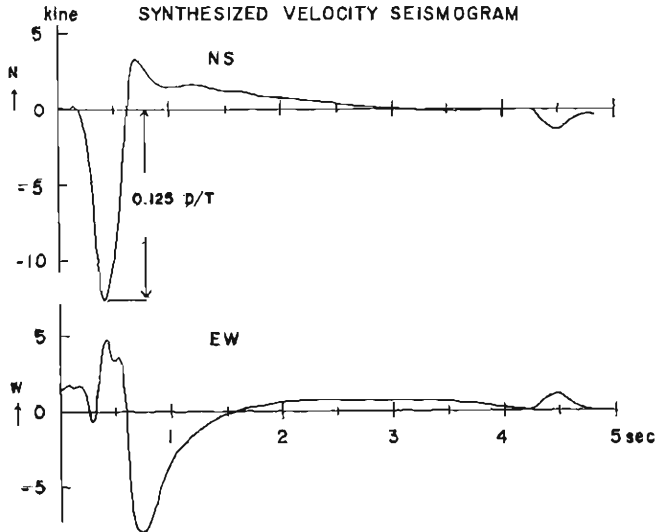


Fig. 18. Synthesized seismograms; NS and EW components. Assumed  $L=7$  km,  $W=3$  km,  $D=26$  cm,  $T=0.26$  sec and a fault direction of  $N 45^\circ W$ .

seismogram does not correspond to the theoretical one. This may be caused by the oversimplification of the theoretical assumption used in this case. In this simplified model, the source is assumed to be unilateral, but this is adopted as a convenience. It will be necessary to consider the effect of ground structure in more detail.

In the observational system the recorder is driven by the starter and no initial motion is recorded, therefore more detailed discussion is difficult.

#### *Source parameters*

Various attempts have been made to find empirical linear relationships between the magnitude  $M$  and the logarithm of one or more of the source parameter (length  $L$ , width  $W$ , dislocation  $D$ ). The following equations are given by Wyss and Brune, and Chinerry<sup>11</sup>), when the magnitude is 3-6 as at Parkfield.

$$M = 1.67 \log LW - 14.51 \quad (8)$$

$$M = 1.32 \log D + 4.27 \quad (9)$$

$$M = 0.79 \log LDW - 4.74 \quad (10)$$

The magnitude of earthquake No. 147 is 4.7, therefore, from eq. (8), we get,

$$LW = 40.37 \text{ km}^2$$

from eq. (9)

$$D = 2.1 \text{ cm}$$

from eq. (10)

$$LDW = 100 \text{ km} \cdot \text{cm}$$

$LDW$  is not equal to the  $LW$  multiplied by  $D$ , and this is because the empirical formulae used are given independently.

Kasahara obtained the seismic moment of the same earthquake from a Love wave at long distance observation (Gifu). Let the moment be  $M_0$ ,  $M_0 = 3.5 \times 10^{22}$  dyne-cm; we then get  $LDW = 35 \text{ km}^2 \cdot \text{cm}$ , since  $M_0 = \mu \cdot LDW$  (by Aki).

In the fault model adopted in this case ( $L = 7 \text{ km}$ ,  $W = 3 \text{ km}$ ), we get  $D = 17 \text{ cm}$  from the value of  $LDW$  obtained by Kasahara. The size of the fault is the maximum value of the buried fault found by Nakamura and Tsuneishi, and hence we should consider  $D \geq 17 \text{ cm}$ .

We assumed a ramp function of  $T = 0.26 \text{ sec}$ , and  $D/T \approx 100 \text{ cm/sec}$  as source time functions, and found good agreement with the observational data. This might be conceived to coincide well with Kasahara's results. The value is less than 1/10 which is given by eq. (9), and is conceived not to be consistent with this case.

## 5. Conclusion

In relation to the source parameters many quantities have not been clarified as yet, hence the model was simplified as a unilateral moving dislocation. And the rough estimation of the surface layer was considered as an amplification factor only. Then

we found fairly good coincidence between the observed values and the theoretical ones as far as the velocity amplitude spectral density are concerned.

From the analyses of the accelerograms near the epicenter it was shown that an estimation of source time function would be possible by the methods described in this paper. A clue of the dependency of the source mechanism on the vibrational characteristics of the ground during strong earthquakes might be found.

However, the synthesized seismograms and the observed ones in the time domain are not precisely consistent because the phase spectra are difficult to consider in both the theoretical and the observed data. That is, the above inconsistency might be caused by the fact that the source model was over-simplified and strict estimation of the effect of the surface layer was very difficult.

It is shown that the source time function of a ramp (duration time  $T=0.26$  sec, slip velocity  $D/T=100\sim 200$  cm/sec) is most preferable when a moving dislocation is assumed. The strong earthquake motion incident to the base will be affected strongly by the source time function.

### Acknowledgments

The authors wish to express their thanks to Dr. M. Shima, Mr. N. Goto and Mr. J. Akamatsu of the Disaster Prevention Research Institute of Kyoto University, for their discussions and co-operations in the preparation of this paper. The data processing was carried out by the use of Facom 230-60, the electronic computer of Kyoto University.

### References

- 1) Schiff, A. and J.L. Bogdanoff: Analysis of Current Methods of Interpreting Strong Motion Accelerograms, *Bull. Seism. Soc. Am.*, 57, 1967, pp. 857-874.
- 2) Hudson, D.E., N.C. Nigam and M.D. Trifunac: Analysis of Strong-Motion Accelerograph Records, *Proc. Fourth World Conf. on Eq. Engr.*, A-2, 1969, pp. 18-25.
- 3) S.E.M.O.C., Earthq. Res. Inst., Tokyo Univ.: Strong Earthquake Motion Records in the Matsushiro Swarm Area, 1967.
- 4) P.W.R.I., Minis. of Construction: Strong-Motion Earthquake Records from Public Works in Japan (The Matsushiro Quake Swarm), 1967.
- 5) Kanai, K., K. Hirano, S. Yoshizawa and T. Asada: Observation of Strong Earthquake Motions in the Mathushiro Area, Part 1. *Bull. Earthq. Inst.*, 44, 1966, pp. 1269-1296.
- 6) Hagiwara, T. and T. and T. Iwata: Summary of the Seismographic Observation of the Matsushiro Swarm Earthquakes, *Bull. Earthq. Res. Inst.*, 46, 1968, pp. 485-515.
- 7) Aki, K.: Seismic Displacements near a Fault, *J. Geophys. Res.* 73, 1968, p. 5319.
- 8) Haskell, N.A.: Elastic Displacements in the Near-Field of a Propagating Fault, *Bull. Seism. Soc. Am.*, 59, 1969, pp. 865-908.
- 9) Brune, J.N.: Tectonic Stress and the Spectra of Seismic Shear Waves from Earthquakes, *J. Geophys. Res.* 75, 1970, pp. 4497-5010.
- 10) Tsuneishi, Y. and K. Nakamura: Faulting Associated with the Matsushiro Swarm Earthquakes, *Bull. Earthq. Res. Inst.*, 48, 1970, pp. 29-52.
- 11) Chinnery, M.A.: Earthquake Magnitude and Source Parameters, *Bull. Seism. Soc. Am.*, 59, 1969, pp. 1969-1982.
- 12) Kasahara, K.: The Source Region of the Matsushiro Swarm Earthquakes. *Bull. Earthq. Res. Inst.*, 48, 1970, pp. 581-602.

- 13) Aki, K. and et al.; Design for Nuclear Power Plants, MIT Press.
- 14) Shima, M.: Characteristics of Vibrations Produced by a Horizontal Point Force in Multilayered Elastic Ground, *Annuals, Disast. Prev. Res. Inst.*, Vol. 13-A, 1970, pp. 197-212.